Iron phosphate nanostructures synthesized by microwave method and their applications in biosensing



2010 Nanotechnology 21 425504

(http://iopscience.iop.org/0957-4484/21/42/425504)

Nanotechnology **21** (2010) 425504 (10pp) doi:10.1088/0957-4484/21/42/425504

# Iron phosphate nanostructures synthesized by microwave method and their applications in biosensing

**Yajing Yin, Hui Zhang, Ping Wu, Bo Zhou[1] and Chenxin Cai[1]**

Jiangsu Key Laboratory of New Power Batteries, Jiangsu Key Laboratory of Biofunctional Materials, Laboratory of Electrochemistry, College of Chemistry and Materials Science, Nanjing Normal University, Nanjing 210097, People's Republic of China

E-mail: zhoubo@njnu.edu.cn and cxcai@njnu.edu.cn

Received 12 July 2010, in final form 25 August 2010
Published 24 September 2010
Online at stacks.iop.org/Nano/21/425504

**Abstract**

A fast, simple microwave heating method has been developed for synthesizing iron phosphate ($FePO_4$) nanostructures. The nanostructures were characterized and confirmed by transmission electronic microscopy (TEM), scanning electronic microscopy (SEM), energy-dispersive x-ray spectroscopy (EDS), x-ray photoelectron spectroscopy (XPS), x-ray powder diffraction (XRD), Fourier transform infrared (FT-IR), and UV–vis spectroscopy. The morphology and the size of the nanomaterials are significantly influenced by the concentration of the precursors and the kinds of surfactants. The nanostructures have been employed as an electrode substrate to immobilize myoglobin (Mb) and to facilitate the direct electron transfer (DET) reaction of the protein. After being immobilized on the nanomaterials, Mb can keep its natural structure and undergo effective DET reaction with a pair of well-defined redox peaks at $-(330 \pm 3.0)$ mV (pH 6.8) and an apparent electron transfer rate constant of 5.54 $s^{-1}$. The Mb–$FePO_4$/GC electrode displays good features in the electrocatalytic reduction of $H_2O_2$, and thus can be used as a biosensor for detecting substrates with a low detection limit ($5 \pm 1$ $\mu$M), a wide linear range (0.01–2.5 mM), a high sensitivity (ca. $85 \pm 3$ $\mu$A $mM^{-1}$ $cm^{-2}$), as well as good stability and reproducibility. Therefore, $FePO_4$ nanomaterials can become a simple and effective biosensing platform for the integration of proteins/enzymes and electrodes, which can provide analytical access to a large group of enzymes for a wide range of bioelectrochemical applications.

## 1. Introduction

Nanostructured materials have received considerable interest because they show physical properties that are significantly different from their bulk materials [1, 2]. Especially, much attention has been focused on inorganic nanomaterials because of their versatile properties, such as optical, electronic, magnetic, catalytic, and electrochemical properties [3–5]. As an important class of inorganic nanomaterials, iron phosphate ($FePO_4$) nanomaterials have attracted considerable research attention for their low cost, environmental friendliness, and biocompatibility. It has been reported that $FePO_4$ exhibits a good catalytic activity toward the oxidation of glycolic acid [6], and methanol [7]. $FePO_4$ has also been shown to have a very high selectivity in oxidative dehydrogenation reactions [8–10]. Wang and Otsuka [11, 12] have reported the exceptional selectivity of $FePO_4$ in methane and ethane oxidation by $O_2$. In particular, $FePO_4$ is a useful electrode material in lithium batteries [13, 14] since it shows a high discharge voltage above 3 V (versus $Li/Li^+$) [15, 16]. To date, $FePO_4$ has been used both as an anode [17, 18] and cathode material [19, 20]. However, to our knowledge, there is no report on using $FePO_4$ nanomaterials to immobilize proteins/enzymes with the aim of achieving a direct electron transfer (DET) reaction for biosensing.

A variety of synthesis methods (soft chemistry, sol–gel, ion-exchange, etc) have been reported for the preparation of nano-sized $FePO_4$ materials [21–23]. However, complex processes and low production rates are common problems to many of these techniques. Recently, Chen [24] reported the

[1] Authors to whom any correspondence should be addressed.

 

synthesis of an array of transition-metal phosphate colloidal spheres by a hydrothermal method. However, the procedure is time consuming. Therefore, a facile and fast solution-based procedure is still highly desirable for preparation of $FePO_4$ nanostructures.

This work reports a facile, inexpensive, and reproducible process for the synthesis of monodispersed $FePO_4$ nanostructures with a size of 50–150 nm using a microwave heating method. The morphology of the synthesized nanostructures depends on a stabilizing agent. In addition, the size of the prepared sample can be easily controlled by adjusting the concentration of the precursor. Compared with the solvothermal method (usually 12 h) [24], the microwave heating method is fundamentally different. The microwave radiation is absorbed and converted to thermal energy, and heat is generated from inside the material. Such an internal rapid heating offers a more homogeneous condition for the reaction and a faster kinetic process. Therefore, the utilization of microwave radiation allows a dramatic reduction of the reaction time (usually less than 10 min) and consumed energy. The reaction rate is enhanced by one to two orders of magnitude [25, 26]. The high specific surface areas and good biocompatibility enable the nanostructures suitable for protein loading and biosensor fabrication. The $FePO_4$ is also used for facilitating the DET reaction of myoglobin (Mb). The characteristics of DET and electrocatalytic features of the immobilized Mb are presented. Therefore, the present work offers a new avenue to synthesize $FePO_4$ nanostructures and widens the applications of $FePO_4$ in electrochemistry and biosensing.

## 2. Experimental details

### *2.1. Chemicals*

Myoglobin (Mb, from horse skeletal muscle, type III, Sigma) was used without further purification. Cetyltrimethylammonium bromide (CTAB), sodium dodecylsulfate (SDS), polyethylene glycol 1000 (PEG-1000), polyethylene glycol 10 000 (PEG-10000), polyvinylpyrrolidone (PVP), ammonium ferrous sulfate hexahydrate ($(NH_4)_2Fe(SO_4)_2{\cdot}6H_2O$), urea, and $H_3PO_4$ were purchased from Shanghai Chemicals Regent Co. Ltd (Shanghai, China) and used as received. The commercial bulk material of iron(III) phosphate dihydrate ($FePO_4{\cdot}2H_2O$) was obtained from Aldrich and used as received. Solutions of $H_2O_2$ were freshly diluted from the 30% solution and their concentrations were determined using a standard solution of $KMnO_4$. 0.1 M phosphate buffer solution (PBS, pH 6.8) was employed as the supporting electrolyte for studying the DET reaction of Mb. All other chemicals were of analytical grade or better and used as received. All solutions were prepared with double-distilled water.

### *2.2. Instruments*

A homemade microwave synthesis system with a maximum output power of 800 W was used for the preparation of the $FePO_4$ nanostructures. The synthesis apparatus was connected with a refluxing system. Scanning electron microscopic (SEM) images of the samples were recorded using a JEOL JSM-5610LV scanning electron microscope (JEOL, Japan). The distribution and the mean particle sizes of the samples were determined by a BI-200SM dynamic light scattering instrument (DLS) (Brookhaven, USA). The x-ray photoelectron spectroscopic (XPS) measurements were made on a ESCALAB 250 spectrometer (Thermo VG Scientific, USA). The binding energy was calibrated using a C 1s photoelectron peak at 284.6 eV as a reference. The x-ray powder diffraction (XRD) patterns of the $FePO_4$ nanomaterials were recorded on a Rigaku/Max-3A x-ray diffractometer with Cu K$\alpha$ radiation ($\lambda = 0.154\,18$ nm). The operational voltage and current were maintained at 40 kV and 40 mA, respectively. Transmission electron microscopic (TEM) images were obtained on a JEOL-2010 microscope with an accelerating voltage of 200 kV. The sample was prepared by sonicating $FePO_4$ in water for 20 min and evaporating one drop of the suspension onto a carbon-coated film supported on a copper grid for TEM measurements. Energy-dispersive x-ray spectroscopy (EDS) was recorded using an attached Oxford Link ISIS energy-dispersive spectrometer fixed to the microscope. The FT-IR spectrum was recorded on a Nexus 670 FT-IR spectrophotometer (Nicolet Instruments) using a KBr disk. UV–vis spectra were recorded using a Cary 5000 UV–vis–NIR spectrophotometer (Varian, USA).

The value of the $\zeta$ potential of the prepared $FePO_4$ nanomaterials was measured with a Zeta potential analyzer (Nano Z, Malvern). The electrochemical experiments were performed with a CHI 660B electrochemical workstation (CH Instruments). The coiled Pt wire and the saturated calomel electrode (SCE) were used as the counter and the reference electrode, respectively. The buffer solution was purged with high purity nitrogen for at least 30 min prior to each experiment and the nitrogen environment was then kept over the solution to prevent oxygen from reaching the solution. All the electrochemical experiments were performed at room temperature ($22 \pm 2\,^{\circ}C$).

### *2.3. Synthesis of $FePO_4$ nanostructures*

All samples were prepared in a microwave system with $(NH_4)_2Fe(SO_4)_2{\cdot}6H_2O$ and $H_3PO_4$ as precursors, CTAB as a stabilizing agent, and urea as a precipitant. The nucleation and growth processes were controlled by adjusting the applied microwave power and the reaction time. In a typical preparation, urea (1.2 g) and CTAB (0.1 g) were dissolved in 40 ml $(NH_4)_2Fe(SO_4)_2{\cdot}6H_2O$ (0.1 mmol) solution, followed by the addition of $H_3PO_4$ (0.1 mmol). The mixture was vigorously stirred until a homogeneous solution was formed. Then the mixture was transferred into a round-bottom flask, and placed in a homemade microwave refluxing synthesis system at 200 W for 6 min. The resulting products were collected by centrifugation, washed sequentially with double-distilled water at least three times, and dried in air at ambient temperature.

To study the influence of the synthetic conditions on the morphology of the $FePO_4$ nanostructures, a variety of surfactants including SDS, PEG-1000, PEG-10000, and

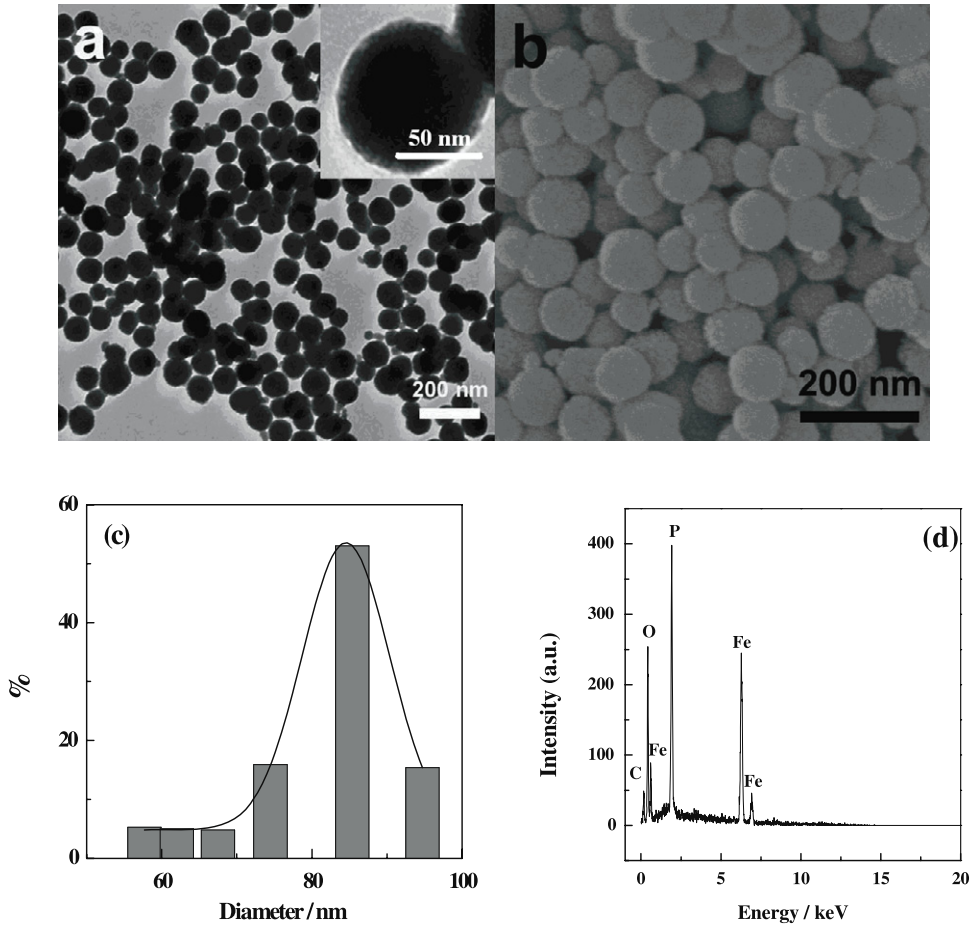


**Figure 1.** Typical TEM image (a), SEM image (b), DLS size-distribution diagram (c), and the EDS spectrum (d) of the as-prepared $FePO_4$ nanomaterials.

PVP, were used as stabilizing agents, respectively. The concentration of $(NH_4)_2Fe(SO_4)_2$ was varied from 1.25 to 5 mM with the concentration of $H_3PO_4$ remaining constant at 2.5 mM. Therefore, the molar ratio of the precursors (the ratio of $(NH_4)_2Fe(SO_4)_2$ to $H_3PO_4$) was varied from 1:2 to 2:1.

### *2.4. Immobilization of Mb and fabrication of Mb–$FePO_4$/GC electrode*

Several parameters were optimized to obtain the best voltammetric response. For the immobilization of the Mb, the glassy carbon electrode (GC, 3 mm in diameter, CH Instruments) was first treated following the procedures reported previously [27]. A 5 $\mu$l dispersion of $FePO_4$ (5 mg $ml^{-1}$), which was prepared by sonicating the nanostructures in water for 30 s, was drop-cast onto the surface of the electrode with a microsyringe. The solvent was allowed to evaporate at room temperature before use (denoted as the $FePO_4$/GC electrode). The Mb was immobilized on the surface of the $FePO_4$ nanomaterials by incubating the $FePO_4$/GC electrode in 2.5 mg $ml^{-1}$ Mb solution (pH 5.0). A preliminary experiment was carried out to establish the time required for reaching the adsorption equilibrium. It was found that the maximum adsorption could be reached within the first few hours and the equilibrium was established within 3–6 h. Therefore, the adsorption experiments were all carried out for 6 h to ensure the equilibrium was reached. During this period Mb was spontaneously adsorbed on the surface of the $FePO_4$ nanomaterials via electrostatic interactions. Mb is positively charged in pH 5.0 PBS since the isoelectric point of the protein is ∼7.2 [28] and the surface of $FePO_4$ has a net negative charge since the value of the $\zeta$ potential of the nanomaterials is ca. −10 mV. The resulting electrode (denoted as the Mb–$FePO_4$/GC electrode) was rinsed with water thoroughly to remove those loosely adsorbed Mb molecules. The electrode was stored at 4 °C when not in use.

Using similar procedures, the Mb/GC electrode was also fabricated. Its DET features and electrocatalytic characteristics were studied and compared with those of the Mb–$FePO_4$/GC electrode.

## 3. Results and discussion

### *3.1. Characterization of $FePO_4$ nanostructures*

The shape and size of the synthesized samples were examined by TEM and SEM. As shown in figures 1(a) and (b), the obtained $FePO_4$ nanomaterials are spherical with a diameter of 80–90 nm. The inset in figure 1(a) clearly shows the surface of the $FePO_4$ nanosphere is not smooth. From the SEM image, it could also be found that the surface of the $FePO_4$

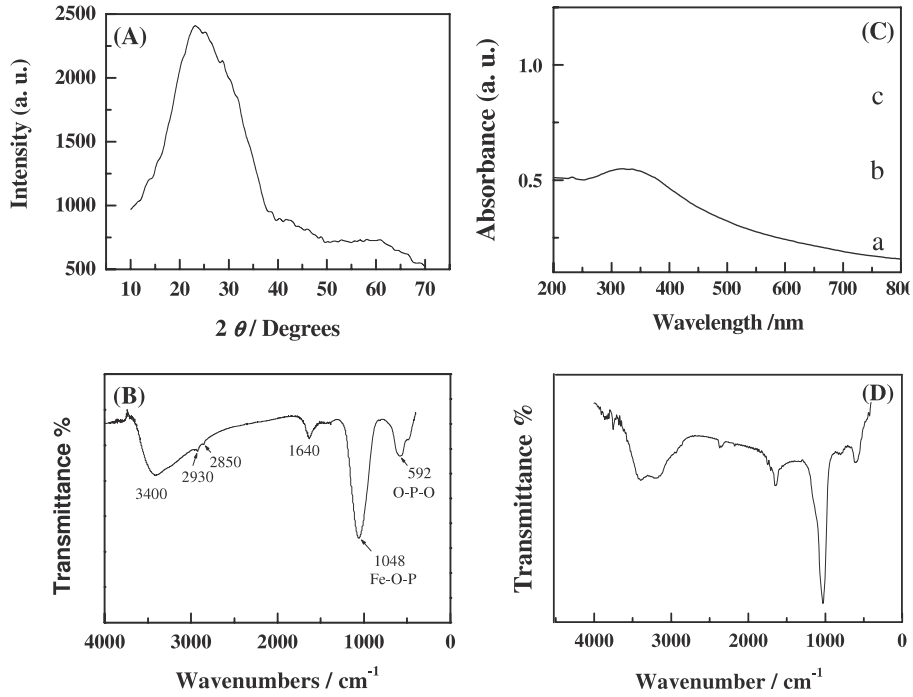


**Figure 2.** XRD patterns (panel (A)), FT-IR (panel (B)), and UV–vis spectra (panel (C)) of the prepared $FePO_4$ nanomaterials. The curve (a)–(c) in panel (C) shows the UV–vis spectra of pure $FePO_4$ (curve (a)), Mb–$FePO_4$ (curve (b)), and Mb in aqueous solution (curve (c), 0.5 mg $ml^{-1}$). Panel (D) shows the FT-IR spectrum of the commercial $FePO_4$ bulk material.

nanosphere is rough, which is constructed by numerous small nanoparticles. This feature is important for the nanomaterials being used for a substrate to immobilize the proteins/enzymes because the high surface area is favorable for the assembly of enzymes. The narrow size distribution of the prepared products is demonstrated by DLS measurement (figure 1(c)). The average diameter of the spheres is about 85 nm, which is in good agreement with the value obtained from the TEM and SEM results. The EDS was recorded to verify the composition of the as-synthesized $FePO_4$ nanomaterials. The results shown in figure 1(d) reveal the presence of iron (6.92, 6.26, and 0.58 keV), phosphorus (1.90 keV), oxygen (0.42 keV), and carbon (1.40 keV). The carbon signal can be attributed to the response of the TEM grid [29]. These results indicate that the obtained nanospheres are composed of iron, phosphorus, and oxygen, which is in agreement with that expected by theory.

The $FePO_4$ nanomaterials were also examined by XRD measurements as shown in figure 2 (panel (A)). A broad peak appears at about 25.0°, indicative of the amorphous features of the prepared product.

Panel (B) in figure 2 depicts the FT-IR spectrum of the prepared $FePO_4$ nanomaterials. The bands at 3400 and 1640 $cm^{-1}$ are ascribed to the vibration of hydroxyl groups. The bands at 592 and 1048 $cm^{-1}$ can be attributed to the asymmetric vibration of the O–P–O [30] and Fe–O–P bond [31], respectively. The IR bands at 2850 and 2930 $cm^{-1}$ are assigned to the characteristic vibration of the $–CH_3$ and $–CH_2–$ group [32] coming from the CTAB molecule, which was used as a stabilizing agent in the synthesis of the $FePO_4$ nanomaterials. The UV spectrum of the nanomaterials is presented in panel (C) of figure 2 (curve (a)). The small band at 230 nm could be assigned to the P–O charge transfer transition and the band at 320 nm to the Fe–O charge transfer transition [33, 34]. Moreover, the IR features of the prepared nanomaterials are consistent with those of commercial bulk $FePO_4$ materials (panel (D), figure 2). These results confirm that the $FePO_4$ nanomaterials have been prepared.

XPS analysis can provide information of the state of the Fe in the $FePO_4$ nanomaterials. The XPS of the $FePO_4$ sample shows peaks for the Fe 2p, Fe 3p, P 2p, P 2s, O 1s, and C 1s core level at a binding energy of 711.0 (Fe 2p), 54.0 (Fe 3p), 133.1 (P 2p), 188.8 (P 2s), 530.9 (O 1s), and 284.6 (C 1s) (panel (A), figure 3), respectively. The binding energy of Fe $2p_{3/2}$ appears at 711.0 eV (panel (B), figure 3); the value is in agreement with that reported for the characteristic of Fe(III) [6]. There is no evidence of Fe(II) existing in samples, because the XPS peak corresponding to Fe(II) should be at 708.2 eV [35]. The values of the binding energy of P $2p_{3/2}$ (133.1 eV, panel (C), figure 3) and O 1s (530.9 eV, panel (D), figure 3) fit well with those reported for the characteristic XPS peaks of the phosphate group [6].

The morphology of the prepared $FePO_4$ samples was significantly influenced by the stabilizing surfactant. As shown in figure 4, in the absence of CTAB, ill-spherical and greatly agglomerated particles (figure 4(a)) are obtained, while in the presence of CTAB, the prepared products have relatively good dispersion with uniform diameters of ∼85 nm (figure 4(b)).

The morphology of the $FePO_4$ sample was also greatly dependent on the kinds of the surfactants being used in the preparation. Figures 4(c)–(f) shows the TEM images of $FePO_4$ samples prepared using SDS (figure 4(c)), PEG-1000 (figure 4(d)), PEG-10000 (figure 4(e)), and PVP (figure 4(f)),

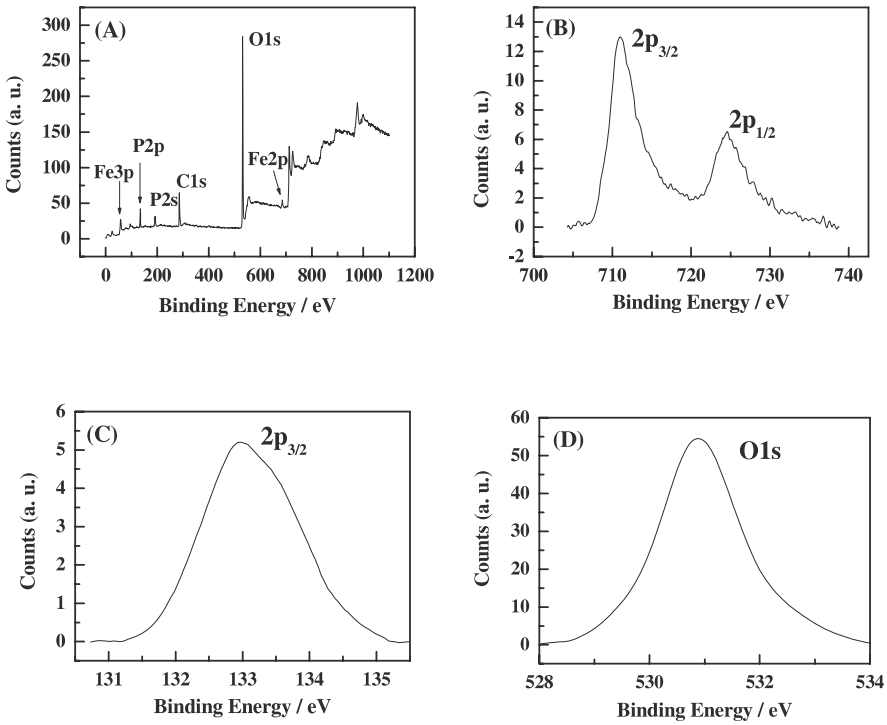


**Figure 3.** XPS spectra of the $FePO_4$ nanomaterials (panel (A)), Fe 2p (panel (B)), P 2p (panel (C)), and O 1s (panel (D)).

respectively, as the stabilizing agent. The morphologies of the $FePO_4$ nanomaterials using these surfactants are totally different from those obtained employing CTAB as the stabilizing agent. They are agglomerated with a size of ca. ∼100 nm except for the small size of the sample produced in the presence of PVP (∼30 nm). These results demonstrate that CTAB plays a crucial role in controlling the spherical morphology of the product, as well as preventing the nanomaterials from aggregating.

As a cationic surfactant, CTAB is an ionic compound that ionizes completely in water [36, 37]. The $CTA^+$ ion is a positively charged tetrahedron with a long hydrophobic tail. Meanwhile the $FePO_4$ nanoparticles are negatively charged as verified by the value of the $\zeta$ potential of the nanomaterials (ca. −10 mV). The $CTA^+$ (cetyltrimethylammonium) ions are adsorbed on the face of nuclei in all the directions to form isotropic growth through electrostatic attraction [38]. Under reflux conditions, these nuclei collide and combine with each other to reduce the surface energy, which helps the aggregation into nanospheres. The shells surrounding the particles are protective layers to prevent nanoparticles from being aggregated into larger particles to a certain extent [38]. Capped by CTAB molecules, these nanospheres remain monodisperse as shown in figure 4(b). In the case of SDS, which is an anionic surfactant, the surfactant molecules cannot be well adsorbed on the face of nuclei due to the electrostatic repulsion, leading to the nanoparticles aggregating into larger particles (figure 4(c)). PEG and PVP are non-ionic surfactants; the stabilization is less effective in comparison with the system stabilized by CTAB. Such an insignificant stabilizing effect can be explained by a weak adsorption on the surface of the $FePO_4$ nanoparticles. The nanoparticles are therefore easily aggregated in the course of their growth (figures 4(d)–(f)).

The morphology of the prepared $FePO_4$ sample is almost independent of the molar ratio of the precursors (the ratio of $(NH_4)_2Fe(SO_4)_2$ to $H_3PO_4$). The spherical $FePO_4$ nanomaterials were obtained by changing the ratio from 1:2 up to 2:1 (figure 5). However, the size of the nanostructures increases with the increase of the ratio of the precursor. As shown in figure 5(a), the nanospheres with average diameters of (50 ± 10) nm are obtained at a molar ratio of 1:2. The average size of the nanomaterials increases to (80 ± 20) and (150 ± 20) nm, respectively, at a molar ratio of 1:1 and 2:1 (figures 5(b) and (c)). This may be due to the high concentration of $(NH_4)_2Fe(SO_4)_2$ accelerating the growth process of the $FePO_4$ nanomaterials resulting in an increase in the size. To verify if the composition of the prepared samples is affected by the concentration of the precursors, the EDS measurements were carried out for $FePO_4$ samples. The results indicated the content of Fe was 31.5, 31.9, and 32.2% for the samples prepared under the molar ratio of the precursors (the ratio of $(NH_4)_2Fe(SO_4)_2$ to $H_3PO_4$) of 1:2, 1:1, and 2:1, respectively, demonstrating that the composition of the prepared nanomaterials is independent of the concentration of the precursors.

### *3.2. DET of Mb immobilized on $FePO_4$ nanostructures*

After the nanomaterials have been completely characterized, we turn to study the immobilization and DET features of Mb on the $FePO_4$ nanostructures to explore the new applicable platform of the materials. Before the voltammetric characteristics of Mb on $FePO_4$ are obtained, UV–vis

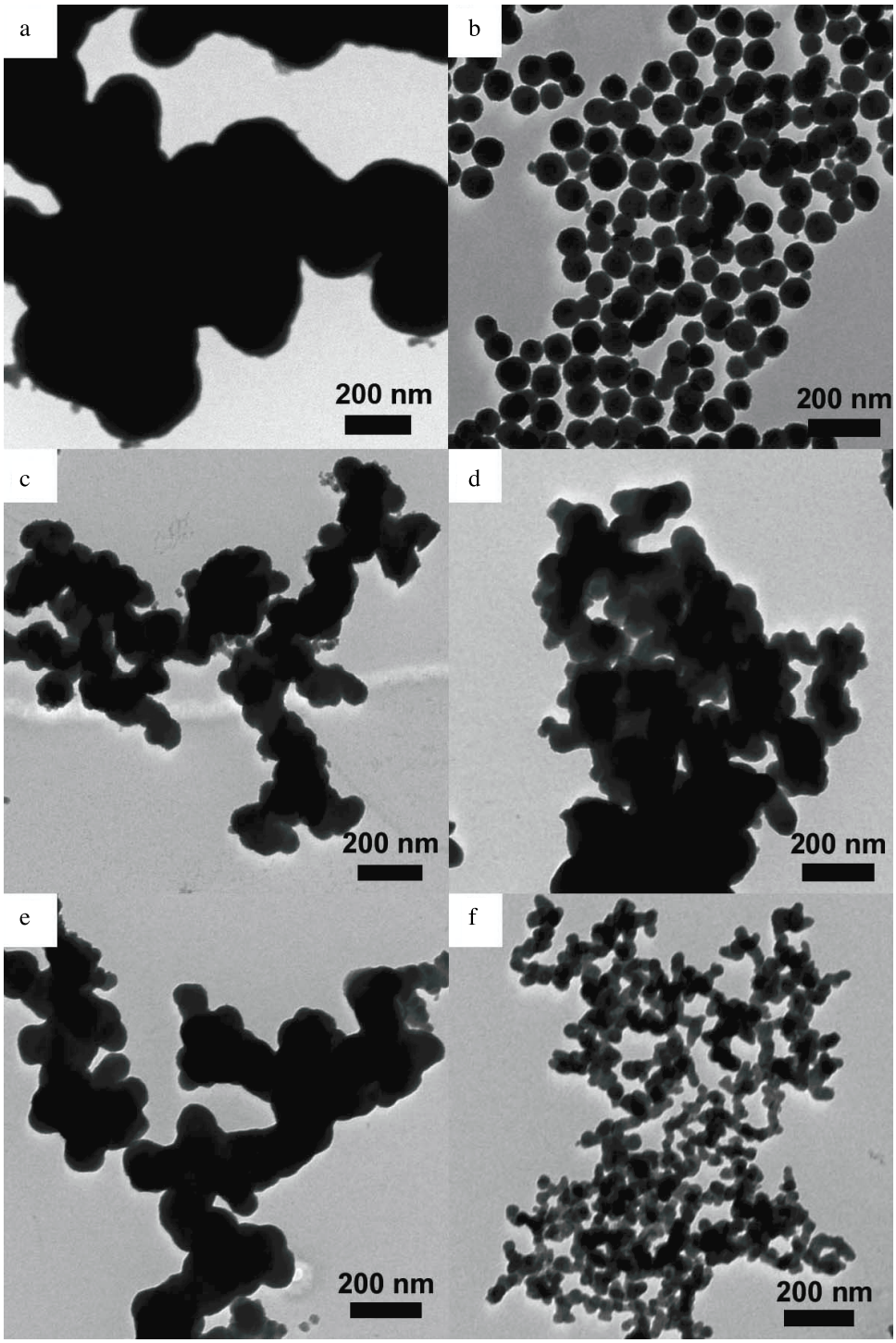


**Figure 4.** TEM images of $FePO_4$ nanomaterials synthesized without (a) and with CTAB (b), SDS (c), PEG-1000 (d), PEG-10000 (e), and PVP (f) as the stabilizing agent, respectively.

spectroscopy is used to confirm that the protein immobilized on the $FePO_4$ surface still retains its native integrated structure because spectroscopy is a useful tool for monitoring possible changes of the Soret absorption band of the heme group. The band shift provides information on the possible denaturation of heme proteins, particularly conformational changes of these proteins [39]. The UV–vis spectrum of Mb–$FePO_4$ is depicted in panel (C) of figure 2 (curve (b)). The peak at 408 nm is attributed to the Soret band of the immobilized Mb, indicating the successful immobilization of Mb on the $FePO_4$ nanomaterials. This immobilization process is completed via the electrostatic interaction between Mb and $FePO_4$ nanomaterials because the surface of $FePO_4$ has a net negative charge, while Mb has a net positive charge at pH 5.0. The features of this peak are identical with those of natural Mb dissolving in solution (408 nm, curve

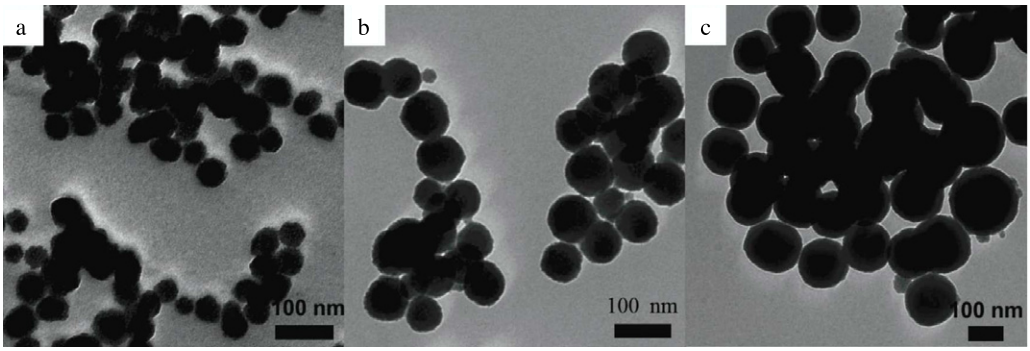


**Figure 5.** TEM images of the $FePO_4$ prepared at a molar ratio of $((NH_4)_2Fe(SO_4)_2$ to $H_3PO_4)$ 1:2 (a), 1:1 (b), and 2:1 (c).

(c)), suggesting no significant denaturation occurred to the protein after it was immobilized onto the surface of the $FePO_4$ nanomaterial. These results also show good biocompatibility of the nanomaterials.

Figure 6 depicts the typical cyclic voltammograms (CV) of the bare GC (curve (a)), $FePO_4$/GC (curve (b)), Mb–$FePO_4$/GC (curve (c)), and Mb/GC electrode (curve (d)) in 0.1 M PBS (pH 6.8) at a scan rate of 100 mV $s^{-1}$. No redox peak is observed at the bare GC and the $FePO_4$/GC electrode in the potential range of interest, indicating that the bare GC and $FePO_4$ nanomaterials cannot be oxidized or reduced in the experimental potential range. The CV of the Mb/GC electrode does not also show any detectable redox peaks (curve (d)), suggesting that Mb cannot undergo an effective DET reaction on the surface of a bare GC electrode. However, a pair of well-defined redox peaks is observed at the Mb–$FePO_4$/GC electrode (curve (c)) with the anodic ($E_{pa}$) and cathodic ($E_{pc}$) peak potentials of ca. −284 and −373 mV, respectively, at a scan rate of 100 mV $s^{-1}$. The formal potential, $E^{0\prime}$, calculated by averaging the value of $E_{pa}$ and $E_{pc}$, is found to be −328.5 mV. This value is close to that previously reported for Mb trapped in polymer films, such as polyacrylamide (−335 mV) [40] or Eastman AQ film (−362 mV) [41], and also similar to those obtained by adsorbing Mb on the surface of clay (−330 mV) [42], carbon nanotubes (−370 mV) [43], and cerium phosphate nanotubes (−(367 ± 3) mV, pH 7.5) [44]. Moreover, it is also similar to those of other heme proteins (enzymes) including hemoglobin [45] and horseradish peroxidase [46–48]. The separation of peak potentials, $\Delta E_p$, is 69 mV, indicating that Mb on $FePO_4$ nanomaterials displays a quasi-reversible electrochemical reaction despite its large molecular structure. These results show that $FePO_4$ nanomaterials can facilitate the effective DET between Mb and the electrode surface, and moreover Mb immobilized on the surface of $FePO_4$ can keep its natural structure. This conclusion is in good agreement with that obtained from UV–vis spectra.

Furthermore, the Mb–$FePO_4$ on the GC electrode surface was fairly stable since the features of the CV of the electrode remained almost unchanged after the electrode was scanned continuously for a long time (100 cycles, at 50 mV $s^{-1}$) in the experimental potential range. In addition, no obvious change was detected after the electrode had been stored in PBS at 4 °C for one week. These characteristics are important when the

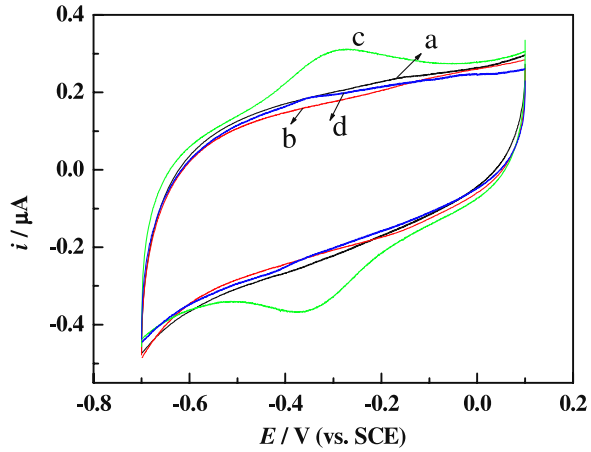


**Figure 6.** Cyclic voltammograms of the GC (a), $FePO_4$/GC (b), Mb–$FePO_4$/GC (c) and Mb/GC (d) electrode in 0.1 M PBS (pH 6.8) at a scan rate of 100 mV $s^{-1}$.

(This figure is in colour only in the electronic version)

electrode is further used as a biosensor for sensing substrates (such as $H_2O_2$, etc).

To investigate the characteristics of Mb adsorbed on the surface of $FePO_4$ nanomaterials, the effects of scan rates on the voltammetric response of the Mb–$FePO_4$/GC electrode were studied in detail (figure 7). As shown in panel (A) of figure 7, almost equal cathodic and anodic peak heights were observed at each scan rate, indicating that all the electroactive ferrous Mb (Mb–Fe(II)), which is produced by the reduction of ferric Mb (Mb–Fe(III)) on the forward scan, can be oxidized to Mb–Fe(III) on the reverse scan. Both the anodic and cathodic peak currents increase linearly with the scan rate up to at least 1000 mV $s^{-1}$ (panel (B), figure 7), which suggests that the redox process is confined to the surface of the electrode, also confirming that the immobilized state of Mb is stable. The $E_{pa}$ and $E_{pc}$ shift slightly to more positive and negative potentials, respectively, with the increase of the scan rate indicating the increase of the electrochemical irreversibility of the DET of the Mb. However, the values of $E^{0\prime}$ (the average value is −(330 ± 3) mV in the scan rate range from 20 to 1000 mV $s^{-1}$) are almost independent of the scan rates. From the dependence of $\Delta E_p$ on the scan rates, the apparent heterogeneous electron transfer rate constant, $k_s$, can be calculated to be 5.54 $s^{-1}$,

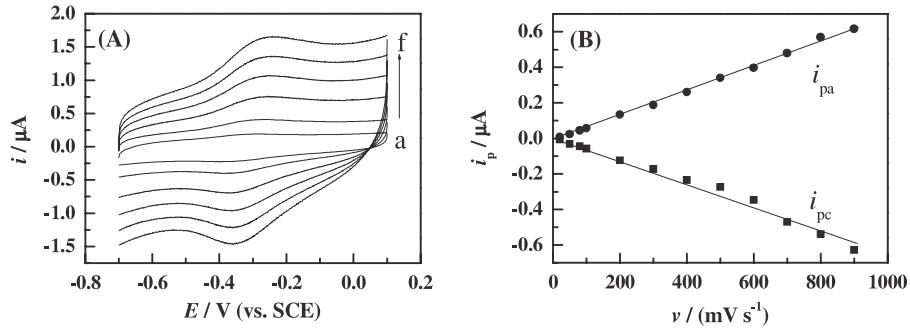


**Figure 7.** Cyclic voltammograms of the Mb–$FePO_4$/GC electrode at scan rates of (from curve (a) to (f)) 50, 100, 200, 300, 400, and 500 mV $s^{-1}$, respectively (panel (A)). The dependence of the anodic and cathodic peak currents on the scan rates (panel (B)).

using the method developed by Laviron [49] for a surface controlled electrochemical system. This value is much higher than those obtained by adsorbing Mb on the surface of carbon nanotubes ($3.11 \pm 0.98$ $s^{-1}$) [43], and bioconjugating Mb with porous nanogranules of zirconium uridine monophosphate, $Zr(UMP)_2{\cdot}H_2O$, ($1.1 \pm 0.3$ $s^{-1}$) [50]. These results indicate that $FePO_4$ nanomaterials can facilitate DET between the adsorbed protein and the electrode surface more effectively.

### *3.3. Effects of solution pH*

It has been reported that the solution pH modulates the accessibility of water molecules to the heme pocket and the protonation of the heme iron-bound histidine in heme proteins, thus affecting the redox potential of these proteins [51]. The cyclic voltammetric characteristics of the Mb–$FePO_4$/GC electrode show a considerable dependence on the pH of the buffer. An increase of the pH in the solution leads to a negative shift in the potential of both the anodic and cathodic peaks (figures 8(a)–(c)). The inset shows the dependence of $E_{pa}$, $E_{pc}$, and $E^{0\prime}$ of the Mb–$FePO_4$/GC electrode on the solution pH. All the $E_{pa}$, $E_{pc}$, and $E^{0\prime}$ have a linear relationship with solution pH with a slope of −48, −45, and −46.5 mV/$pH^{-1}$ units, respectively, in the range of 5.0–9.0. These values are very close to those obtained by Meng *et al* at the CeP/GC electrode (−47 mV/$pH^{-1}$) [44], Li *et al* at the $\{clay/Mb\}_6$ electrode (−42.4 mV/$pH^{-1}$) [42], Cao *et al* at the gold nanoparticle/carbon nanotube nanohybrid film electrode (−42.2 mV/$pH^{-1}$) [52] and Lü *et al* at the carbon nanotube electrode (−43.7 mV/$pH^{-1}$) [43]. However, they are quite different from the theoretical value of −58.6 mV/$pH^{-1}$ at 22 °C for a reversible electron transfer reaction coupled with an equal number of protons and electrons. The reason for this difference cannot be fully understood at present, but it has probably resulted from the influence of the protonation states of amino acids near the heme and protonation of the water molecules coordinated to the heme iron [53]. This influence leads to more complex reaction mechanisms of the electron transfer process between the electrode and the protein, in which the ratio of the number of protons to the number of electrons is more complicated. The microenvironment of Mb at the surface of the electrode may significantly influence the detailed mechanism of the DET of the protein. The overall reaction of the DET of Mb at $FePO_4$ may include several fundamental

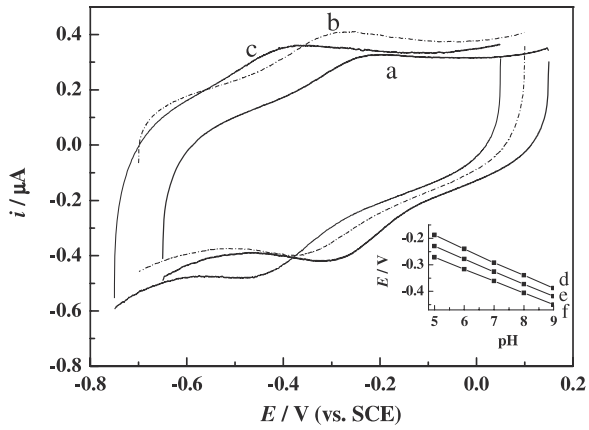


**Figure 8.** Cyclic voltammograms of the Mb–$FePO_4$/GC electrode in 0.1 M PBS at a pH of 5.0 (a), 7.0 (b), and 9.0 (c). The scan rate is 100 mV $s^{-1}$. The inset shows the dependence of $E_{pa}$ (d), $E_{pc}$ (e), and $E^{0\prime}$ (f) on the solution pH.

steps, and some steps correspond to the transfer of one or more protons. Thus, it is not surprising that the total number of electrons and protons involved in the overall reaction is not equal. Nevertheless, the pH-dependent peak potential in figure 8 indicates that the electron transfer between the protein and the electrode is indeed accompanied by proton transfer.

### *3.4. Electrocatalysis of Mb*

It was reported that heme proteins (enzymes), such as cytochrome *c*, hemoglobin, Mb, etc, usually have good electrocatalytic activities toward the reduction of $O_2$, trichloroacetic acid, $H_2O_2$, etc [27, 54]. Having demonstrated the DET characteristics of the Mb–$FePO_4$/GC electrode, the electrocatalytic reduction of $H_2O_2$ was studied at the Mb–$FePO_4$/GC electrode by cyclic voltammetry, as shown in figure 9. In the absence of $H_2O_2$, a pair of redox peaks of Mb is observed figure 9(a), which is similar to that depicted in figure 6(c). However, in the presence of 0.1 mM of $H_2O_2$, the voltammetric features of the electrode change significantly. A large cathodic current of the reduction of $H_2O_2$ appears at ca. −420 mV and the anodic peak decreases (figure 9(b)) compared with those of figure 9(a). The onset potential (at ca. −200 mV) is 170 mV more

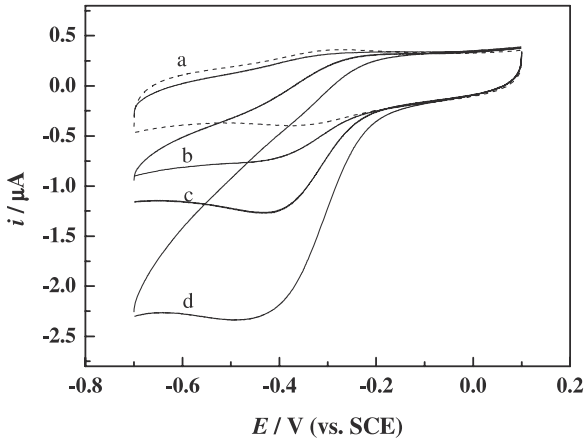


**Figure 9.** Cyclic voltammetric responses of the Mb–$FePO_4$/GC electrode in PBS (pH 6.8) in the absence (a) and presence of 0.1 (b), 0.2 (c), and 0.5 mM (d) $H_2O_2$. The scan rate is 100 mV $s^{-1}$.

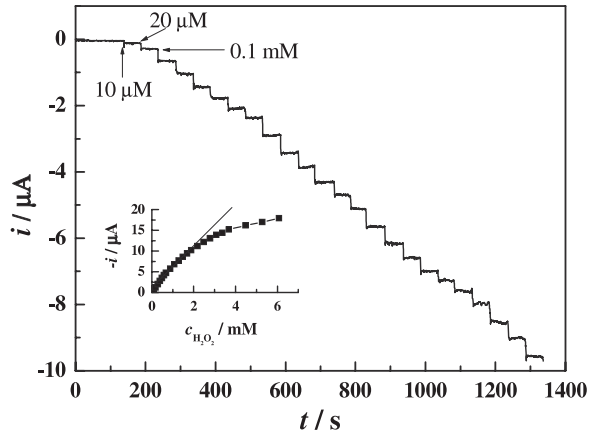


**Figure 10.** Amperometric responses of the Mb–$FePO_4$/GC electrode to the successive addition of $H_2O_2$ in PBS (0.1 M, pH 6.8) at an applied potential of −450 mV. The inset shows the dependence of the response of the electrode on the $H_2O_2$ concentration.

positive than the reduction peak actually appears. The electrocatalytic cathodic currents are enhanced significantly by a further increase of the concentration of $H_2O_2$ in the solution (figures 9(c) and (d)). These characteristics are the typical features of electrocatalytic reactions. The controlled experimental results demonstrate that the $FePO_4$/GC electrode has a very low electrocatalytic activity toward the reduction of $H_2O_2$ only at a potential below −650 mV (not shown here), suggesting that the reduction of $H_2O_2$ shown in figures 10(b)–(d) mainly comes from the electrocatalysis of Mb. These results indicate that Mb immobilized on $FePO_4$ nanomaterials keeps intrinsic and good electrocatalytic activities towards its substrates. The biocompatibility of $FePO_4$ enables the nanomaterial to become a good biosensing platform for realizing direct electrochemistry and electrocatalysis of heme-containing proteins/enzymes.

Figure 10 depicts the typical amperometric response of the Mb–$FePO_4$/GC electrode to the successive addition of $H_2O_2$ in solution at a detection potential of −450 mV, which was selected from the hydrodynamic voltammogram (not shown here). Immediately after the addition of $H_2O_2$, the response increases and reaches 95% of the steady-state value within 2 s. The results suggest that the Mb–$FePO_4$/GC electrode responds rapidly to the change of the substrate concentration. The electrode linearly responds to $H_2O_2$ at a lower concentration and attains saturation level at a higher concentration as expected for the Michaelis–Menten characteristic (the inset of figure 10). The apparent Michaelis–Menten constant ($K_M^{app}$) is estimated to be ca. 0.4 mM from the Lineweaver–Burk plot (not shown here), indicating a good biocompatibility of $FePO_4$ nanostructures. The response displays a good linear range from 0.01 to 2.5 mM with a correlation coefficient of 0.992 and a slope of (5.9 ± 0.2) $\mu$A $mM^{-1}$. Therefore, the sensitivity is evaluated to be ca. (85 ± 3) $\mu$A $mM^{-1}$ $cm^{-2}$. The detection limit is estimated to be ca. (5 ± 1) $\mu$M at a signal/noise (S/N) of three. The linear response range is wider than those of 4–124, 3.92–180.14, 24.2–167, 1–42, 2–160, 6–160, 2.5–50 $\mu$M reported previously by immobilizing Mb at a hexagonal mesoporous silica matrix [55], at a porous nanogranule of $Zr(UMP)_2{\cdot}H_2O$ [50], at single-walled carbon nanotube (SWCNT)–cetyltrimethylammonium bromide (CTAB) nanocomposites [56], at $TiO_2$-coated multiwalled carbon nanotubes (MWCNTs) [57], at titanate nanotubes [58], at carbon ionic liquid (CIL) electrodes [59], and $Al_2O_3$ nanoparticle modified electrodes [60], respectively. The value of the detection limit obtained in this work is similar to that acquired at clay–chitosan–gold nanoparticle nanohybrid (7.5 $\mu$M) [61], SWCNT–CTAB nanocomposite (8 $\mu$M) [56], Nafion–MWCNT–CIL (6.0 $\mu$M) [62], and MWCNT (4.2 $\mu$M) [63] electrodes, and is much lower than the 55 and 75 $\mu$M reported for the triacetone triperoxide composite carbon paste [64] and NiO nanoparticle modified electrodes [65], respectively. Therefore, it can be concluded that Mb–$FePO_4$ presents a good analytical performance in the determination of $H_2O_2$.

All these features indicate that Mb immobilized on the $FePO_4$ nanomaterials keeps intrinsic and good electrocatalytic activities towards its substrate. The biocompatibility of the nanomaterial enables it to become a good biosensing platform for realizing direct electrochemistry and electrocatalysis of heme-containing proteins/enzymes.

Additional experiments were conducted to test the reproducibility and stability of the Mb–$FePO_4$/GC electrode toward the reduction of $H_2O_2$. Five different and freshly prepared electrodes were employed to detect the reduction of $H_2O_2$ in concentrations of 0.01–2.5 mM. The RSD (relative standard deviation) is 2.6% estimated from the slopes of five calibration curves (a calibration curve for each electrode). The assay precision of the electrode was examined by ten determinations at a $H_2O_2$ concentration of 1 mM. A RSD of 3.5% is obtained. These reveal an acceptable reproducibility and precision in the construction of the electrode. No obvious change in the response was found after the electrode was immersed in solution and stored at 4 °C for 10 h. The electrode can retain ca. 90% of its initial response to 1 mM $H_2O_2$ within two weeks. The higher stability can be attributed to the capability of the $FePO_4$ nanospheres immobilizing Mb molecules and retaining their biological activities.

## 4. Conclusions

In summary, we have developed an economical and efficient microwave-assisted method for the synthesis of iron phosphate ($FePO_4$) nanospheres. The morphology and size of the product are found to strongly depend on the surfactant and the concentration of the precursor. The $FePO_4$ nanospheres have been employed as substrates for the immobilization of a heme protein, Mb. After being immobilized on the surface of $FePO_4$ nanospheres, Mb can still retain its natural structure and undergo an effective direct electron transfer reaction with a pair of well-defined, quasi-reversible redox peaks in its CV. The electrode displays good features in the electrocatalytic reduction of hydrogen peroxide, and thus can be used as a biosensor for detecting substrates with good reproducibility and stability.

## References


[1] Lee K J, Oh J H, Kim Y and Jang J 2006 *Chem. Mater.* **18** 5002
[2] Liu J, Li X and Dai L 2006 *Adv. Mater.* **18** 1740
[3] Capek I 2004 *Adv. Colloid Interface Sci.* **110** 49
[4] Cao Z, Jiang W Q, Ye X Z and Gong X L 2008 *J. Magn. Magn. Mater.* **320** 1499
[5] Zhai Y A, Zhang Q, Liu F Q and Gao G 2008 *Mater. Lett.* **62** 4563
[6] Wang X, Wang Y, Tang Q, Guo Q, Zhang Q and Wan H 2003 *J. Catal.* **217** 457
[7] Klissurski D, Rives V, Abadzhjieva N, Pesheva Y, Pomonis P, Sdovkos T and Petrakis D 1993 *J. Chem. Soc. Chem. Commun.* 1606
[8] Ai M and Ohdhan K 1997 *Appl. Catal.* **150** 13
[9] Miller J E 2002 *Appl. Catal.* A **231** 281
[10] Ai M 2002 *Appl. Catal.* A **234** 235
[11] Wang Y and Otsuka K 1995 *J. Catal.* **155** 256
[12] Wang Y and Otsuka K 1997 *J. Catal.* **171** 106
[13] Masquelier C, Reale P, Wurm C, Morcrette M, Dupont L and Larcher D 2002 *J. Electrochem. Soc.* **149** A1037
[14] Delacourt C, Poizot P, Morcrette M, Tarascon J M and Masquelier C 2004 *Chem. Mater.* **16** 93
[15] Zaghib K and Julien C M 2005 *J. Power Sources* **142** 279
[16] Prosini P P, Lisi M, Scaccia S, Carewska M, Cardellini F and Pasquali M 2002 *J. Electrochem. Soc.* **149** A297
[17] Son D, Kim E, Kim T G, Kim M G, Cho J and Park B 2004 *Appl. Phys. Lett.* **85** 5875
[18] Kalaiselvi N, Doh C H, Park C W, Moon S I and Yun M S 2004 *Electrochem. Commun.* **6** 1110
[19] Padhi A K, Nanjundaswamy K S and Goodenough J B 1997 *J. Electrochem. Soc.* **144** 1188
[20] Cui W J, Liu H J, Wang C X and Xia Y Y 2008 *Electrochem. Commun.* **10** 1587
[21] Baies R, Pralong V, Caignaert V and Raveau B 2006 *Mater. Res. Bull.* **41** 1170
[22] Kahoul A and Hammouche A 2010 *Ionics* **16** 105
[23] Nicolas M, Laurence C, Dany C, Lydie B and Pierre K 2010 *Chem. Mater.* **22** 1854
[24] Chen C, Chen W, Lu J, Chu D R, Huo Z Y, Peng Q and Li Y D 2009 *Angew. Chem. Int. Edn* **48** 1
[25] Sertkol M, Köseoglu Y, Baykal A, Kavas H and Toprak M S 2010 *J. Magn. Magn. Mater.* **322** 866
[26] Rao K J, Vaidhyanathan B, Ganguli M and Ramakrishnan P A 1999 *Chem. Mater.* **11** 882
[27] Du P, Liu S N, Wu P and Cai C X 2007 *Electrochim. Acta* **52** 6534
[28] Enoki Y, Ohga Y, Kawase M and Nakatani A 1984 *Biochim. Biophys. Acta* **789** 334
[29] Zhang L, Cao X F, Ma Y L, Chen X T and Xue Z L 2010 *Cryst. Eng. Commun.* **12** 207
[30] Shi Z C, Attia A, Ye W L, Wang Q, Li Y X and Yang Y 2008 *Electrochim. Acta* **53** 2665
[31] Mal N K, Bhaumik A, Matsukata M and Fujiwara M 2006 *Indust. Eng. Chem. Res.* **45** 7748
[32] Yu D H, Wu C, Kong Y, Xue N H, Guo X F and Ding W P 2007 *J. Phys. Chem.* C **111** 14394
[33] Yuan Q, Zhang Q and Wang Y 2005 *J. Catal.* **233** 221
[34] Nagaraju P, Lingaiah N, Balaraju M and Sai Prasad P S 2008 *Appl. Catal.* A **339** 99
[35] Cataldi T R, De Benedtto G E and Bianchini A J 1998 *J. Electroanal. Chem.* **448** 111
[36] Wang S L, Xu H, Qian L Q, Jia X, Wang J W, Liu Y Y and Tang W H 2009 *J. Solid State Chem.* **182** 1088
[37] Yan T, Zhang D, Shi L, Yang H, Mai H and Fang J 2009 *Mater. Chem. Phys.* **117** 234
[38] Yang J, Quan Z W, Kong D Y, Liu X M and Lin J 2007 *Cryst. Growth Des.* **7** 730
[39] Chi Z and Asher S A 1998 *Biochemistry* **37** 2865
[40] Shen L, Huang R and Hu N 2002 *Talanta* **56** 1131
[41] Hu N and Rusling J F 1997 *Langmuir* **13** 4119
[42] Li Z and Hu N 2003 *J. Electroanal. Chem.* **558** 155
[43] Lü Y F, Yin Y J, Wu P and Cai C X 2007 *Acta Phys.-Chim. Sin.* **23** 5
[44] Meng L, Yang L G, Zhou B and Cai C X 2009 *Nanotechnology* **20** 035502
[45] Cai C X and Chen J 2004 *Anal. Biochem.* **325** 285
[46] Sun D, Cai C X, Li X, Xing W and Lu T H 2004 *J. Electroanal. Chem.* **566** 415
[47] Zhao G C, Yin Z Z, Zhang L and Wei X W 2005 *Electrochem. Commun.* **7** 256
[48] Cai C X and Chen J 2004 *Acta Chim. Sin.* **62** 335
[49] Laviron E 1979 *J. Electroanal. Chem.* **101** 19
[50] Qiao Y, Jian F and Bai Q 2008 *Biosens. Bioelectron.* **23** 1244
[51] Lei C, Wollenberger U, Bistolas N, Guiseppi-Elie A and Scheller F W 2002 *Anal. Bioanal. Chem.* **372** 235
[52] Cao W, Wei C, Hu J and Li Q 2008 *Electroanalysis* **20** 1925
[53] Liu H, Tian Z, Lu Z, Zhang Z, Zhang M and Pang D 2004 *Biosens. Bioelectron.* **20** 294
[54] Lu X, Hu J, Yao X, Wang Z and Li J 2006 *Biomacromolecules* **7** 975
[55] Dai Z H, Xu X X and Ju H X 2004 *Anal. Biochem.* **332** 23
[56] Wang S, Xie F and Liu G 2009 *Talanta* **77** 1343
[57] Zhang L, Tian D B and Zhu J J 2008 *Bioelectrochemistry* **74** 157
[58] Liu A H, Wei M D, Honma I and Zhou H S 2005 *Anal. Chem.* **77** 8068
[59] Shangguan X and Zheng J 2009 *Electroanalysis* **21** 881
[60] Guo W, Lu H Y and Hu N F 2006 *Electrochim. Acta* **52** 123
[61] Zhao X J, Mai Z B, Kang X H, Dai Z and Zou X Y 2008 *Electrochim. Acta* **53** 4732
[62] Sun W, Li X, Wang Y, Li X, Zhao C and Jiao K 2009 *Bioelectrochemistry* **75** 170
[63] Zhao G C, Zhang L and Wei X W 2004 *Anal. Biochem.* **329** 160
[64] Jian F F, Qiao Y B, Yu H Q and Zhuang R R 2007 *Anal. Lett.* **40** 2664
[65] Moghaddam A B, Ganjali M R, Dinarvandb R, Ahadi S and Saboury A 2008 *Biophys. Chem.* **134** 25